mately 60° at one-half power, directed to the west, was employed. The radar was approximately 76 m above the sea so that line-of-sight propagation conditions existed. Each spectrum is the result of about 1000 seconds of observation. The spectra are computed by using digital techniques. Four range intervals, corresponding to a region from about 10 to 40 km from the radar, have been summed to improve the statistics of the spectra. It is of extreme interest that, when examined individually, the echo spectra from these four range intervals are indistinguishable in their primary features. Further smoothing is obtained by taking a running average in frequency over 5-mhz intervals. Unfortunately, the wave-height spectrum of the sea was not available, but when swell was present its period could be estimated from the waves breaking on the beach. In Figs. 1 and 2 the largest echoes correspond to waves moving toward the transmitter. However, negatively shifted Doppler features are always present. In each figure, the approximate noise level of the system is indicated by the bold line to the right of the echoes. The frequency stability of the system is such that the echoes from stationary targets (arrow) were not resolved in frequency, even before the frequency smoothing. In both figures, the first-order Bragg lines themselves show considerable broadening. The points indicated $\pm f_B$ correspond to the theoretical positions of the first-order Bragg lines. It should also be noted that these lines may be shifted significantly, up to about 30 mhz, from their theoretical positions. The causes of this broadening are undetermined; currents along the California coast are of sufficient magnitude to account for the observed shifts.

The spectrum of Fig. 1 is interpreted as arising from a wind-driven sea, in the absence of significant swell. The central feature, indicated by the arrow, is a residual echo from stationary objects and is at the transmitter frequency. Power spectral densities above the system noise level, including the region around the transmitted frequency line, represent scattering from the sea. The spectrum is nonsymmetrical about the Bragg line. We estimate the slope of the spectrum in the region immediately above $+f_B$ to be -40 decibels per hertz; below $+f_B$ the magnitude of positive slope may be twice as great. The overall features of this spectrum are as predicted by Barrick (*6*) and agree quite well with his published theoretical spectra. However, detailed quantitative comparisons, which are quite complex, have not yet been carried out.

Figure 2 is interpreted as arising from a sea surface containing significant long-period components. The frequency displacements of the distinct features in the sidebands about the Bragg lines correspond to modulation with a 17-second period. This period agrees with that of the waves breaking on the beach, as determined with a watch. Modulation sidebands from other swell with a shorter period may also be present. Well-developed, smooth sidebands such as those in Fig. 1 are absent.

These spectra are typical of our observations to date. Significant sideband energy is always present; the nature of the sidebands varies from day to day. In Fig. 1, approximately 50 percent of the total echo signal above the transmitter line is contained in the sidebands. In both figures, the rather well-defined minima on either side of the principal Bragg lines are indicative of a minimum in ocean wave energy at periods of the order of 15 to 20 seconds. We conclude that second-order wave-wave interactions, as first suggested by Hasselmann (*2*), do occur and that they are observable. The more detailed calculations of Barrick (*6*) account for the observed features of the spectra. From the variation of the sidebands with time over a period of 1 day, we conclude that these sidebands are quite sensitive to the total wave-height spectrum of the ocean, as has been suggested. Consequently, it seems likely that decameter radar will be able to provide measurements of the sea state. This has not previously been possible because of the technical difficulties of carrying out observations with the frequency resolution and dynamic range of those described here.

G. LEONARD TYLER
WILLIAM E. FAULKERSON
ALLEN M. PETERSON
CALVIN C. TEAGUE
Center for Radar Astronomy, Stanford University, Stanford, California 94305

References and Notes

1. D. D. Crombie, *Nature* **175**, 681 (1955).
2. K. Hasselmann, *Nature Phys. Sci.* **229**, 16 (1971).
3. ———, *Rev. Geophys.* **4**, 1 (1966).
4. J. F. Ward, *Nature* **223**, 1325 (1969).
5. S. O. Rice, *Commun. Pure Appl. Math.* **4**, 351 (1951).
6. D. E. Barrick, in *Remote Sensing of the Troposphere*, V. Derr, Ed. (Government Printing Office, Washington, D.C., 1972), chap. 12.
7. O. M. Phillips, *The Dynamics of the Upper Ocean* (Cambridge Univ. Press, London, 1966).
8. This work was carried out at the Stanford Center for Radar Astronomy as part of a joint study with Scripps Institute of Oceanography. Financial support for this work is provided by Scripps Institute of Oceanography under ARPA contract N00014-69-A-0200-6012.

17 April 1972; revised 7 June 1972

Sea Level at Southern California: A Decadal Fluctuation

Abstract. *The winter mean height of sea level at southern California rose 5.6 centimeters between the periods 1948–1957 and 1958–1969. These periods correspond to two fairly coherent large-scale climatic regimes with different air-sea coupling, which were previously identified. The rise was mainly due to a change in the thermohaline structure of the water as a result of changes in prevailing winds.*

Winters in the decade of the 1960's were anomalously cold over the eastern United States but warmer than normal over the Far West (*1*). This short-period climatic fluctuation was attributed to an amplified atmospheric long-wave pattern in which a strong trough (equatorward bulge in the upper westerlies) dominated the central Pacific. The downstream response to this feature was a strong ridge in western North America and a strong trough in the East. Subsequently, Komhyr *et al.* (*2*) related observed increases in total ozone during the 1960's to this anomalous pattern. It was suggested (*1*) that this anomalous circulation pattern may have been forced by anomalous temperatures at the surface of the sea in the North Pacific.

Further studies of this regime (*3*) and the regime of the preceding decade indicate that an abrupt transition occurred in about 1957–1958 between radically different winter patterns of atmospheric circulation and temperature. An example of this break between two coherent regimes is the winter temperature in Atlanta, Georgia, which averaged 3°C colder in the later period than in the earlier.

Because of the large winter differences in mean pressure gradient and sea surface temperature off the West Coast in these roughly decadal periods, as shown in Fig. 1, we considered a

priori that the height of sea level in winter along the West Coast might also have reflected a decadal difference. Indeed it did, as shown by observations at San Diego (Fig. 2), where the sea level in the winter (December through February) in the later period averaged 5.6 cm higher than in the earlier period. A similar rise was observed at Los Angeles (not shown). This difference was found to be highly significant (*4*).

Although thorough explanations of the "climate" of sea level have been given (*5*) and studies of long-period trends in sea level have often appeared (*6, 7*), comparatively little work has been done on the subject of sea level variations on decadal time scales. In attempting to account for the variation described above we have considered the following causes enumerated by Montgomery (*8*):

1) Changes in atmospheric pressure.

2) Dynamic effects of ocean currents.

3) Local wind effects.

4) Thermohaline effects.

5) Long-period astronomic tides.

6) Local additions to water mass.

7) Changes in bathymetric configurations.

8) Glacial melt and land subsidence.

Item 1 was easily calculated from hydrostatic considerations by using barometric pressures in San Diego and the "inverted barometer" method. Items 2, 3, and 4 are only partially separable, each contributing a share of the overall dynamic effect. All major transport components, namely Ekman, baroclinic, and barotropic, were calculated from atmospheric and oceanographic data. The difference between the total transport and the sum of baroclinic and Ekman transports accounts for the sea level inclination caused by barotropic current and wind effect on water piling up along the coast. However, item 4 has also been treated independently by computing the anomaly of geopotential on the basis of steric considerations, which involve the expansion and contraction of water columns as a result of density variations. We can neglect item 5 because it contributes only a minute part of the sea level fluctuation and the effect on the decadal difference is very small (*5*). Items 6 and 7 can be neglected in this area. Item 8 has been accounted for by computing the long-period secular rising trend of the sea level at San Diego since 1926. For the data sources and details of the analysis and computations see (*9*).

The results of these computations indicate that atmospheric pressure differences (the inverted barometer effect of item 1) account for 0.6 cm, the overall dynamic effect for 1.0 cm, and the secular rise (item 8) for 1.0 cm, while the thermohaline effect (item 4) accounts for 3.7 cm. The net computed rise, 6.3 cm, compares favorably with the observed rise of 5.6 cm. By far the largest effect is thermal: the surface layer of the ocean off the coast averaged up to 1°C warmer in the later period than in the earlier one. This warming was associated with less north-to-south wind stress (stronger anomalous southwest wind components) in the later decade, which in turn resulted in more eastward oceanic flow from the subtropics and less southward flow from the California current system. Figure 1 shows the differences between periods (later minus earlier) in the sea level pressure and also in the sea surface temperature.

Such coupled air-sea anomalies could account for that part of long-term trends in sea level which cannot be explained by river runoff, glacial melt, and land subsidence. These trends have been studied along the East Coast and

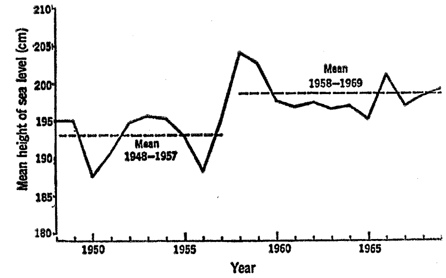

Fig. 2. Winter (December through February) mean height of sea level (in centimeters above an arbitrary reference level) at San Diego, California (*12*).

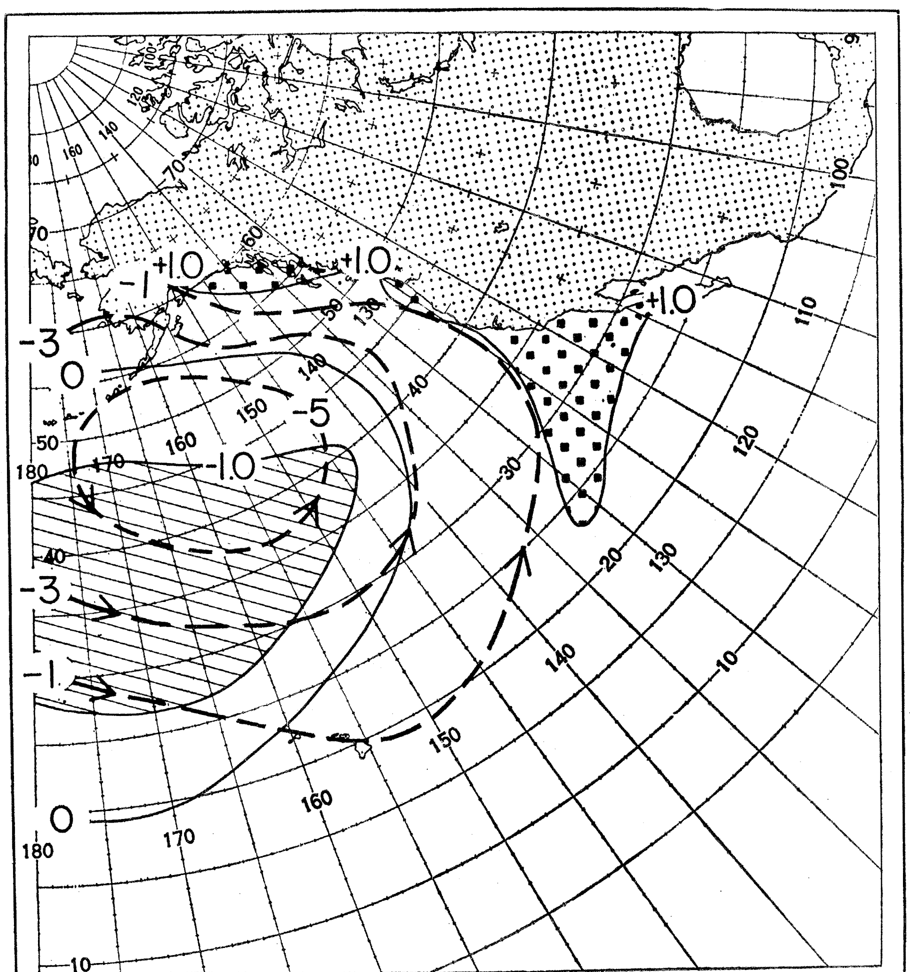

Fig. 1. Differences between the winter (December through February) sea surface temperature changes (drawn for intervals of 1.0°C) (solid lines) and sea level pressure changes (in millibars) (broken lines) of 1948–1957 and 1958–1969 (later minus earlier period). The hatched area denotes negative changes greater than 1°C, the area marked with filled squares positive changes greater than 1°C. Arrows indicate the directional change in geostrophic air flow.

the Gulf Coast of the United States by Hicks (*6*) and Meade and Emery (*7*) and along the West Coast by Roden (*10*) and Saur (*11*).

JEROME NAMIAS
JOSEPH CHI KAN HUANG
Scripps Institution of Oceanography, La Jolla, California 92037

References and Notes

1. J. Namias, *Science* **170**, 741 (1970).
2. W. D. Komhyr, E. W. Barrett, G. Slocum, H. K. Weickmann, *Nature* **232**, 390 (1971).
3. J. Namias, in *Proceedings of the 20th Nobel Symposium* (Almqvist & Wiksell, Uppsala, Sweden, in press).
4. A test was made of the hypothesis that the 1948–1957 winter seasons (December through February) were from the same population as the 1958–1969 winter seasons. The Student's *t*-test was applied to the specific hypothesis that the means of these two periods were equal, their variances were equal, and the population variance could be estimated from their sample variances. The t value was 4.44, highly significant at 20 degrees of freedom ($t_{.995} = 2.84$). Thus, we must discard the possibility that the samples are from the same population and accept the difference between periods as real.
5. J. Pattullo, W. Munk, R. Revelle, E. Strong, *J. Mar. Res.* **14**, 88 (1955).
6. S. D. Hicks, *Shore Beach*, in press.
7. R. H. Meade and K. O. Emery, *Science* **173**, 425 (1971).
8. R. B. Montgomery, *J. Mar. Res.* **1**, 165 (1937).
9. J. C. K. Huang, *J. Phys. Oceanogr.*, in press.
10. G. I. Roden, *J. Geophys. Res.* **71**, 4755 (1966).
11. J. F. T. Saur, *ibid.* **67**, 2781 (1962).
12. The data are from the tide gauge records of the Coast and Geodetic Survey, now the National Ocean Survey, National Oceanic and Atmospheric Administration, Rockville, Maryland.

20 April 1972; revised 30 May 1972

Rare-Earth Oxides of Manganese and Cobalt Rival Platinum for the Treatment of Carbon Monoxide in Auto Exhaust

Abstract. *The perovskite-like compounds $RE_{1-x}Pb_xMnO_3$ and $RECoO_3$, where RE (rare earth) is lanthanum, praseodymium, or neodymium, are active catalysts for the oxidation of carbon monoxide. Crushed single crystals of these compounds compare favorably with commercial platinum catalysts in initial activity and lifetime. Therefore, these compounds are promising substitutes for platinum in devices for the catalytic treatment of auto exhaust.*

Recently, mixed oxides of cobalt, namely, $La_{0.8}Sr_{0.2}CoO_3$ and $LaCoO_3$, have been described as active catalysts for electrode oxidation-reduction reactions (*1*) and hydrogenation reactions (*2*), respectively. It has been suggested that $LaCoO_3$ might be a good catalyst for the treatment of auto exhaust gases (*2*). We have tested this compound, and others with the same perovskite-like crystal structure, in the oxidation of CO, the main toxic constituent of automotive exhaust. The compounds $LaCoO_3$ and $PrCoO_3$ were found to be active catalysts for the oxidation of CO. The manganites $La_{1-x}Pb_xMnO_3$ and $Pr_{1-x}Pb_xMnO_3$, but particularly $Nd_{1-x}Pb_xMnO_3$, with $0.4 < x < 0.6$, were very active also. The presence of Pb in these compounds led us to measure the poisoning of the activity by Pb derived from gasoline additives. This was not as severe a problem as with other catalysts. The cobaltites and manganites compare favorably with commercial Pt catalysts, which were tested under the same conditions (Table 1). They show initial activities similar to that of the PTX catalyst (Engelhard), which was designed for exhaust treatment (*3*). The activities of the manganites deteriorate considerably more slowly than that of Pt. Therefore, these compounds seem very promising substitutes for Pt in catalytic devices for the treatment of auto exhaust.

The test reaction was the oxidation of CO with O_2. In a continuous flow system a mixture of CO and O_2 (2 : 1 molar ratio) was fed (30 ml/min) through a charge of approximately 2 cm^3 of catalyst. The effluent from the reactor was automatically sampled at intervals of 2 minutes or more, and analyzed by means of a gas-liquid chromatograph with an automatic integrator. The conversion of CO was determined as a function of temperature while the catalyst was slowly heated up. The activities of the fresh catalysts are given in Table 1 as the temperatures at which 5, 10, or 20 percent conversion of CO was reached, normalized for a 3-g charge of catalyst. The deactivation of the catalysts with time was subsequently followed at constant temperature (Table 1). The

Table 1. Activity and lifetime of oxidation catalysts for the test reaction: $CO + \frac{1}{2}O_2 \rightarrow CO_2$. Flow rate: 30 ml/min of a stoichiometric mixture at normal temperature and pressure.

Catalyst*	S‡ (m^2/g)	Activity test†				Life test			
		Weight of catalyst (g)	Temperature (°C) for CO conversion of			Time (hours)	Temperature (°C)	Conversion§	
			5%	10%	20%			Beginning (%)	End (%)
Pt (PTX)	7.0	1.2	185	205	225	77	235	11	5.9
Pt (PTX)	7.0	0.91	177	197	222	56	235	8.5	6.4
Pt (0.5% on Al_2O_3)	110	0.94	80	160					
$La_{1-x}Pb_xMnO_3$ (sample 1)	< 0.1	2.8	190	215	245				
$La_{1-x}Pb_xMnO_3$ (sample 2)	< 0.1	5.1	183	205	233	136	330	68	44
$Pr_{1-x}Pb_xMnO_3$	< 0.1	3.5	198	225	247				
$Nd_{1-x}Pb_xMnO_3$	< 0.1	3.4	165	180	195	60	208	22	13
$LaCoO_3$ (sample 1)	< 0.1	4.4	180	200					
$LaCoO_3$ (sample 1)	< 0.1	3.7	183	196	215	15	210	20	6.5
$LaCoO_3$ (sample 2)	< 0.1	5.6	187	197	208	25	200	18	9.3
$LaCoO_3$ (sample 2)	< 0.1	4.6	190						
$PrCoO_3$	< 0.1	3.7	160	175		60	212	16	11

* The atomic fraction x in the manganites may vary between 0.4 and 0.6. All oxides listed are crushed single crystals. † Conversions are normalized for 3 g of catalyst, on the assumption that the reaction rate is first order with respect to CO and O_2. At these relatively low conversions, the error involved is slight. ‡ Specific surface area was determined with the Shell/Perkin-Elmer Sorptionmeter. From the size of the single crystal particles, a specific surface area of 0.03 m^2 per gram of catalyst was calculated for the rare-earth oxides. § Conversions at the beginning and end of the test are for the actual weight of charge in column 3.